the human iPS-HLCs as compared with cryopreserved human hepatocytes. In fact, cryopreserved human hepatocytes expressed human *ALB* at an approximately 50-fold higher level than the human iPS-HLCs (**Fig. 2C**), even if the gene expression levels of human *ALB* in the human iPS-HLCs were up-regulated after transplantation (**Fig. 3**). Although the gene expression levels of human *ALB* in the human iPS-HLCs might be up-regulated over the long-term, both LacZ- and FNK-mice became weak at 4 weeks after transplantation in the present study. These results suggest that the transplanted human iPS-HLCs could not support the liver functions of recipient mice, because the hepatic functions of the human iPS-HLCs were lower than those of cryopreserved human hepatocytes. Therefore, more technical improvements in generating mature iPS-HLCs will be needed in order to generate human liver chimeric mice with fully functional human-type livers. Incidentally, we sacrificed the mice at 4 weeks after transplantation in this study. However, it would be interesting to observe these mice for longer than 4 weeks.

Interestingly, we observed significant increases in the expression levels of human hepatocyte-related genes in the human iPS-HLCs of FNK-mice as compared with the Ad-FNK-transduced human iPS-HLCs before transplantation (**Fig. 3**). This finding may have been due to aspects of the *in vivo* liver environment, such as the interaction with other cells, functional polarity, and extracellular matrix. In a future study, it would be intriguing to isolate human iPS-HLCs from a transplanted mouse liver and use them for drug toxicity screening *in vitro*. Because previous studies have shown that human pluripotent stem cell-derived pancreatic cells were maturated and differentiated into functional β-cells at least 3 months after transplantation into mice (13), further maturation of the human iPS-HLCs might be expected at longer times (over 4 weeks) after transplantation. It has been shown that human hepatocytes repopulated in the livers of mice can be serially transplanted into the livers of other mice and survive (2). The repopulation efficacy of serially transplanted mice was increased as compared with that in the initially transplanted mice (2). Therefore, serial transplantation of the human iPS-HLCs might enhance the repopulation efficacy.

In this study, we succeeded in enhancing the repopulation efficiency of human liver chimeric mice generated by transplantation of the Ad-FNK-transduced human iPS-HLCs into uPA/SCID mice. Our method using ectopic expression of FNK should be useful to generate chimeric mice with a high level of human liver chimerism. To the best our knowledge, the human ALB secretion levels and repopulation efficacy in our chimeric mice with human iPS-HLCs were higher than those in the mice used in previous reports, although improvements are required to generate chimeric mice with

fully functional human-type livers.

Acknowledgements

We thank Misae Nishijima, Reiko Hirabayashi, Natsumi Mimura, and Nobue Hirata for their excellent technical support. We also thank Katsuhiro Kanda (Hitachi High-Technologies Corp.) for providing nanopillar~~nanopilar~~ plates and Shigeo Ohta (Nippon Medical School) for providing *FNK* gene. HM and KK were supported by grants from the Ministry of Health, Labor, and Welfare of Japan. HM was also supported by the Japan Research Foundation for Clinical Pharmacology. FS was supported by Program for Promotion of Fundamental Studies in Health Sciences of the National Institute of Biomedical Innovation. YN and KT (K. Takayama) were supported by a Grant in-aid for JSPS Fellows.

1. Asoh, S.; Ohtsu, T.; Ohta, S. The super anti-apoptotic factor Bcl-xFNK constructed by disturbing intramolecular polar interactions in rat Bcl-xL. J. Biol. Chem. 275(47):37240-37245; 2000.
2. Azuma, H.; Paulk, N.; Ranade, A.; Dorrell, C.; Al-Dhalimy, M.; Ellis, E.; Strom, S.; Kay, M. A.; Finegold, M.; Grompe, M. Robust expansion of human hepatocytes in Fah-/-/Rag2-/-/Il2rg-/- mice. Nat. Biotechnol. 25(8):903-910; 2007.
3. Bissig, K. D.; Wieland, S. F.; Tran, P.; Isogawa, M.; Le, T. T.; Chisari, F. V.; Verma, I. M. Human liver chimeric mice provide a model for hepatitis B and C virus infection and treatment. J. Clin. Invest. 120(3):924-930; 2010.
4. de la Coste, A.; Fabre, M.; McDonell, N.; Porteu, A.; Gilgenkrantz, H.; Perret, C.; Kahn, A.; Mignon, A. Differential protective effects of Bcl-xL and Bcl-2 on apoptotic liver injury in transgenic mice. Am. J. Physiol. 277(3 Pt 1):G702-708; 1999.
5. Frisch, S. M. Evidence for a function of death-receptor-related, death-domain-containing proteins in anoikis. Curr. Biol. 9(18):1047-1049; 1999.
6. Gupta, S.; Rajvanshi, P.; Sokhi, R.; Slehria, S.; Yam, A.; Kerr, A.; Novikoff, P. M. Entry and integration of transplanted hepatocytes in rat liver plates occur by disruption of hepatic sinusoidal endothelium. Hepatology 29(2):509-519; 1999.
7. Hasegawa, M.; Kawai, K.; Mitsui, T.; Taniguchi, K.; Monnai, M.; Wakui, M.; Ito, M.; Suematsu, M.; Peltz, G.; Nakamura, M.; Suemizu, H. The reconstituted 'humanized liver' in TK-NOG mice is mature and functional. Biochem. Biophys. Res. Commun. 405(3):405-410; 2011.
8. He, Z.; Zhang, H.; Zhang, X.; Xie, D.; Chen, Y.; Wangensteen, K. J.; Ekker, S. C.; Firpo, M.; Liu, C.; Xiang, D.; Zi, X.; Hui, L.; Yang, G.; Ding, X.; Hu, Y.; Wang, X. Liver xeno-repopulation with human hepatocytes in Fah-/-Rag2-/- mice after pharmacological immunosuppression. Am. J. Pathol. 177(3):1311-1319; 2010.
9. Hiraga, N.; Imamura, M.; Abe, H.; Hayes, C. N.; Kono, T.; Onishi, M.; Tsuge, M.; Takahashi, S.; Ochi, H.; Iwao, E.; Kamiya, N.; Yamada, I.; Tateno, C.; Yoshizato, K.; Matsui, H.; Kanai, A.; Inaba, T.; Tanaka, S.; Chayama, K. Rapid emergence of telaprevir resistant hepatitis C virus strain from wildtype clone in vivo. Hepatology 54(3):781-788; 2011.
10. Inamura, M.; Kawabata, K.; Takayama, K.; Tashiro, K.; Sakurai, F.; Katayama, K.; Toyoda, M.; Akutsu, H.; Miyagawa, Y.; Okita, H.; Kiyokawa, N.; Umezawa, A.; Hayakawa, T.; Furue, M. K.; Mizuguchi, H. Efficient generation of hepatoblasts from human ES cells and iPS cells by transient overexpression of homeobox gene HEX. Mol. Ther. 19(2):400-407; 2011.
11. Kawabata, K.; Sakurai, F.; Yamaguchi, T.; Hayakawa, T.; Mizuguchi, H. Efficient

gene transfer into mouse embryonic stem cells with adenovirus vectors. Mol. Ther. 12(3):547-554; 2005.

12. Koizumi, N.; Mizuguchi, H.; Utoguchi, N.; Watanabe, Y.; Hayakawa, T. Generation of fiber-modified adenovirus vectors containing heterologous peptides in both the HI loop and C terminus of the fiber knob. J. Gene Med. 5(4):267-276; 2003.
13. Kroon, E.; Martinson, L. A.; Kadoya, K.; Bang, A. G.; Kelly, O. G.; Eliazer, S.; Young, H.; Richardson, M.; Smart, N. G.; Cunningham, J.; Agulnick, A. D.; D'Amour, K. A.; Carpenter, M. K.; Baetge, E. E. Pancreatic endoderm derived from human embryonic stem cells generates glucose-responsive insulin-secreting cells in vivo. Nat. Biotechnol. 26(4):443-452; 2008.
14. Lamothe, B.; Aggarwal, B. B. Ectopic expression of Bcl-2 and Bcl-xL inhibits apoptosis induced by TNF-related apoptosis-inducing ligand (TRAIL) through suppression of caspases-8, 7, and 3 and BID cleavage in human acute myelogenous leukemia cell line HL-60. J. Interferon Cytokine Res. 22(2):269-279; 2002.
15. Maizel, J. V., Jr.; White, D. O.; Scharff, M. D. The polypeptides of adenovirus. I. Evidence for multiple protein components in the virion and a comparison of types 2, 7A, and 12. Virology 36(1):115-125; 1968.
16. Miki, T.; Ring, A.; Gerlach, J. Hepatic differentiation of human embryonic stem cells is promoted by three-dimensional dynamic perfusion culture conditions. Tissue engineering. Part C, Methods 17(5):557-568; 2011.
17. Mitchell, C.; Mallet, V. O.; Guidotti, J. E.; Goulenok, C.; Kahn, A.; Gilgenkrantz, H. Liver repopulation by Bcl-x(L) transgenic hepatocytes. Am. J. Pathol. 160(1):31-35; 2002.
18. Mizuguchi, H.; Kay, M. A. Efficient construction of a recombinant adenovirus vector by an improved in vitro ligation method. Hum. Gene Ther. 9(17):2577-2583; 1998.
19. Mizuguchi, H.; Kay, M. A. A simple method for constructing E1- and E1/E4-deleted recombinant adenoviral vectors. Hum. Gene Ther. 10(12):2013-2017; 1999.
20. Mizuguchi, H.; Koizumi, N.; Hosono, T.; Utoguchi, N.; Watanabe, Y.; Kay, M. A.; Hayakawa, T. A simplified system for constructing recombinant adenoviral vectors containing heterologous peptides in the HI loop of their fiber knob. Gene Ther. 8(9):730-735; 2001.
21. Nagamoto, Y.; Tashiro, K.; Takayama, K.; Ohashi, K.; Kawabata, K.; Sakurai, F.; Tachibana, M.; Hayakawa, T.; Furue, M. K.; Mizuguchi, H. The promotion of hepatic maturation of human pluripotent stem cells in 3D co-culture using type I collagen and Swiss 3T3 cell sheets. Biomaterials 33(18):4526-4534; 2012.
22. Rytomaa, M.; Martins, L. M.; Downward, J. Involvement of FADD and caspase-8

signalling in detachment-induced apoptosis. Curr. Biol. 9(18):1043-1046; 1999.

23. Sainz, B., Jr.; Barretto, N.; Martin, D. N.; Hiraga, N.; Imamura, M.; Hussain, S.; Marsh, K. A.; Yu, X.; Chayama, K.; Alrefai, W. A.; Uprichard, S. L. Identification of the Niemann-Pick C1-like 1 cholesterol absorption receptor as a new hepatitis C virus entry factor. Nat. Med. 18(2):281-285; 2012.

24. Sato, Y.; Yamada, H.; Iwasaki, K.; Tateno, C.; Yokoi, T.; Yoshizato, K.; Horii, I. Human hepatocytes can repopulate mouse liver: histopathology of the liver in human hepatocyte-transplanted chimeric mice and toxicologic responses to acetaminophen. Toxicol. Pathol. 36(4):581-591; 2008.

25. Sharma, M. R.; Dworakowski, W.; Shapiro, B. H. Intrasplenic transplantation of isolated adult rat hepatocytes: sex-reversal and/or suppression of the major constituent isoforms of cytochrome P450. Toxicol. Pathol. 40(1):83-92; 2012.

26. Takahashi, K.; Tanabe, K.; Ohnuki, M.; Narita, M.; Ichisaka, T.; Tomoda, K.; Yamanaka, S. Induction of pluripotent stem cells from adult human fibroblasts by defined factors. Cell 131(5):861-872; 2007.

27. Takayama, K.; Inamura, M.; Kawabata, K.; Katayama, K.; Higuchi, M.; Tashiro, K.; Nonaka, A.; Sakurai, F.; Hayakawa, T.; Furue, M. K.; Mizuguchi, H. Efficient generation of functional hepatocytes from human embryonic stem cells and induced pluripotent stem cells by HNF4alpha transduction. Mol. Ther. 20(1):127-137; 2012.

28. Takayama, K.; Inamura, M.; Kawabata, K.; Sugawara, M.; Kikuchi, K.; Higuchi, M.; Nagamoto, Y.; Watanabe, H.; Tashiro, K.; Sakurai, F.; Hayakawa, T.; Furue, M. K.; Mizuguchi, H. Generation of metabolically functioning hepatocytes from human pluripotent stem cells by FOXA2 and HNF1alpha transduction. J. Hepatol. 57(3):628-636; 2012.

29. Takayama, K.; Inamura, M.; Kawabata, K.; Tashiro, K.; Katayama, K.; Sakurai, F.; Hayakawa, T.; Furue, M. K.; Mizuguchi, H. Efficient and directive generation of two distinct endoderm lineages from human ESCs and iPSCs by differentiation stage-specific SOX17 transduction. PloS one 6(7):e21780; 2011.

30. Takayama, K.; Kawabata, K.; Nagamoto, Y.; Kishimoto, K.; Tashiro, K.; Sakurai, F.; Tachibana, M.; Kanda, K.; Hayakawa, T.; Furue, M. K.; Mizuguchi, H. 3D spheroid culture of hESC/hiPSC-derived hepatocyte-like cells for drug toxicity testing. Biomaterials 34(7):1781-1789; 2013.

31. Takehara, T.; Tatsumi, T.; Suzuki, T.; Rucker, E. B., 3rd; Hennighausen, L.; Jinushi, M.; Miyagi, T.; Kanazawa, Y.; Hayashi, N. Hepatocyte-specific disruption of Bcl-xL leads to continuous hepatocyte apoptosis and liver fibrotic responses. Gastroenterology 127(4):1189-1197; 2004.

32. Tashiro, K.; Kondo, A.; Kawabata, K.; Sakurai, H.; Sakurai, F.; Yamanishi, K.; Hayakawa, T.; Mizuguchi, H. Efficient osteoblast differentiation from mouse bone marrow stromal cells with polylysin-modified adenovirus vectors. Biochem. Biophys. Res. Commun. 379(1):127-132; 2009.

33. Tateno, C.; Yoshizane, Y.; Saito, N.; Kataoka, M.; Utoh, R.; Yamasaki, C.; Tachibana, A.; Soeno, Y.; Asahina, K.; Hino, H.; Asahara, T.; Yokoi, T.; Furukawa, T.; Yoshizato, K. Near completely humanized liver in mice shows human-type metabolic responses to drugs. Am. J. Pathol. 165(3):901-912; 2004.

34. Thomson, J. A.; Itskovitz-Eldor, J.; Shapiro, S. S.; Waknitz, M. A.; Swiergiel, J. J.; Marshall, V. S.; Jones, J. M. Embryonic stem cell lines derived from human blastocysts. Science 282(5391):1145-1147; 1998.

35. Tzung, S. P.; Fausto, N.; Hockenbery, D. M. Expression of Bcl-2 family during liver regeneration and identification of Bcl-x as a delayed early response gene. Am. J. Pathol. 150(6):1985-1995; 1997.

36. Vosough, M.; Omidinia, E.; Kadivar, M.; Shokrgozar, M. A.; Pournasr, B.; Aghdami, N.; Baharvand, H. Generation of functional hepatocyte-like cells from human pluripotent stem cells in a scalable suspension culture. Stem cells and development 22(20):2693-2705; 2013.

37. Woo, D. H.; Kim, S. K.; Lim, H. J.; Heo, J.; Park, H. S.; Kang, G. Y.; Kim, S. E.; You, H. J.; Hoeppner, D. J.; Kim, Y.; Kwon, H.; Choi, T. H.; Lee, J. H.; Hong, S. H.; Song, K. W.; Ahn, E. K.; Chenoweth, J. G.; Tesar, P. J.; McKay, R. D.; Kim, J. H. Direct and indirect contribution of human embryonic stem cell-derived hepatocyte-like cells to liver repair in mice. Gastroenterology 142(3):602-611; 2012.

38. Yoshikawa, T.; Niwa, T.; Mizuguchi, H.; Okada, N.; Nakagawa, S. Engineering of highly immunogenic long-lived DC vaccines by antiapoptotic protein gene transfer to enhance cancer vaccine potency. Gene Ther. 15(19):1321-1329; 2008.

Figure legends

Figure 1

FNK shows an enhanced anti-apoptotic activity in human iPS-HLCs against various death stimuli.

(A) The procedure for differentiation of human iPS cells (Dotcom) into the HLCs via mesendoderm cells, definitive endoderm cells, and hepatoblasts is presented schematically. In the hepatic differentiation, not only the addition of growth factors but also stage-specific transient transduction of both FOXA2- and HNF1α-expressing Ad vectors (Ad-FOXA2 and Ad-HNF1α, respectively) were performed. The cellular differentiation procedure is described in detail in the Materials and Methods section. The human iPS-HLCs were transduced with Ad-LacZ or Ad-FNK on day 34. (B) The gene expression levels of *ALB* and *CYP3A4* were measured by real-time RT-PCR on day 35. On the y axis, the gene expression levels in PHs (three lots of PHs were used), which were cultured for 48 hr after plating (PHs-48hr), were taken as 1.0. (C) The amount of ALB secretion was examined in Ad-LacZ-transduced human iPS-HLCs, Ad-FNK-transduced human iPS-HLCs, and PHs-48hr. (D) On day 35, the efficiency of hepatocyte differentiation was measured by estimating the percentage of ASGR1-positive cells using FACS analysis. (E) The cell viability was counted on day 35. (F, G) Ad-LacZ-transduced human iPS-HLCs or Ad-FNK-transduced human iPS-HLCs were incubated with Staurosporine (an inhibitor of protein kinase C; 40 nM) (F) or calcium ionophore A23187 (2 μM) (G), and then surviving cells were counted by trypan blue exclusion. The amount of surviving cells on day 0 was taken as 1.0. All data are represented as means ± SD (n=3). $^{**}P<0.01$.

Figure 2

The human ALB concentration in the mouse blood was increased by the transplantation of Ad-FNK-transduced human iPS-HLCs.

Human iPS cells (Dotcom) were differentiated into the HLCs as described in **Figure 1A**. (A) The Ad-LacZ- or Ad-FNK-transduced human iPS-HLCs (1×10^6 cells) were transplanted into uPA/SCID mice by intrasplenic injection. After the injection of the cells, the mice spleens were excised. The experimental schedule is presented schematically. (B) Human ALB concentrations in the mouse blood were monitored once a week. Triangles and squares represent LacZ-mice (n=10) and FNK-mice (n=12), respectively ~~(n=10 and 12)~~. (C) The gene expression level of human *ALB* in the human iPS-HLCs, which exist in the liver of LacZ-mice and FNK-mice, was

measured by real-time RT-PCR at 4 weeks after transplantation (LacZ-mice (*n*=3) and FNK-mice (*n*=4), respectably). The whole livers of LacZ-mice or FNK-mice, not isolated human iPS-HLCs, were used in this analysis. Undifferentiated human iPS cells (Dotcom; iPS (*n*=3)) and cryopreserved human hepatocytes (CHH (*n*=3)), which were harvested just after thawing, were used as a control ~~(*n* = 3 and 4)~~. All data are represented as means ± SE. **P*<0.05. n.s.; not significant.

Figure 3

The hepatocyte-related gene expression levels of the human iPS-HLCs were enhanced in the mouse liver.

Human iPS cells (Dotcom) were differentiated into the HLCs as described in **Figure 1A**. The Ad-FNK-transduced human iPS-HLCs (1 x 10^6 cells) were transplanted into uPA/SCID mice by intrasplenic injection as described in **Figure 2A**. At 4 weeks after transplantation, the gene expression levels of human hepatocyte-related markers, such as human *ALB*, human *αAT*, human *ASGR1*, human *HNF4α*, human *CYP3A4*, human *CYP2D6*, human *CYP7A1*, human *CYP3A5*, human *UGT1A1*, human *UGT1A3*, human *FXR*, and human *PXR*, were measured in the human iPS-HLCs, which were ~~recovered~~ fromin the liver of FNK mice (post-transplantation (*n*=4)), by real-time RT-PCR. The whole livers of FNK-mice, not isolated human iPS-HLCs, were used in this analysis. On the y axis, the gene expression levels in the Ad-FNK-transduced human iPS-HLCs before transplantation (pre-transplantation (*n*=3)) were taken as 1.0. All data are represented as means ± SE ~~(*n*=3 and 4)~~.

Figure 4

The repopulation efficiencies in the chimeric mice were up-regulated by the transplantation of Ad-FNK-transduced human iPS-HLCs.

Human iPS cells (Dotcom) were differentiated into the HLCs as described in **Figure 1A**. The Ad-LacZ- or Ad-FNK-transduced human iPS-HLCs (1 x 10^6 cells) were transplanted into uPA/SCID mice by intrasplenic injection as described in **Figure 2A**. (A-C) At 4 weeks after transplantation, chimeric mouse livers were analyzed by immunohistochemical staining. Clusters of human ALB- (A) and human αAT- (B) and human CK8/18-expressing cells (C) were found in liver sections. Scale bars represent 100 μm. (D) The repopulation efficiencies in the LacZ-mice (*n*=7) and FNK-mice (*n*=8) were calculated by the ratio of human αAT-expressing areas to the total liver section area. All data are represented as means ± SE ~~(*n*=7 and 8)~~. ***P*<0.01.

Table 1

Gene Symbol	Primers (forward/reverse; 5' to 3')
human GAPDH	TTGAGGTCAATGAAGGGGTC/GAAGGTGAAGGTCGGAGTCA
human ALB	TTACCAAAGTCCACACGGAATG/CGCCCTGTCATCAGCACAT
human CYP3A4	AAGTCGCCTCGAAGATACACA/AAGGAGAGAACACTGCTCGTG
human αAT	ACTGTCAACTTCGGGGACAC/CATGCCTAAACGCTTCATCA
human ASGR1	CATAGGCCCTGTGAACACCT/GCCTTGTCCAGCTCTGTCTC
human HNF4α	CGTCATCGTTGCCAACACAAT/GGGCCACTCACACATCTGTC
human CYP2D6	CTTTCGCCCCAACGGTCTC/TTTTGGAAGCGTAGGACCTTG
human CYP3A5	CGGCATCATAGGTAGGTGGT/TATGAACTGGCCACTCACCC
human UGT1A1	TGACGCCTCGTTGTACATCAG/GGCACAGGGTACGTCTTCAAG
human UGT1A3	TCAACTGTGCCAACAGGAAG/CTGAGACCATTGATCCCAAAG
human FXR	CACAGCGTTTTTGGTAATGC/TTGTTTGTGGAGACAGAGCCT
human PXR	TCCGGAAAGATCTGTGCTCT/AGGGAGATCTGGTCCTCGAT

Table 2

Gene Symbol	Assay ID for Taqman gene expression assays
human GAPDH	Hs99999905_m1
human CYP3A4	Hs00430021_m1
human CYP7A1	Hs00167982_m1

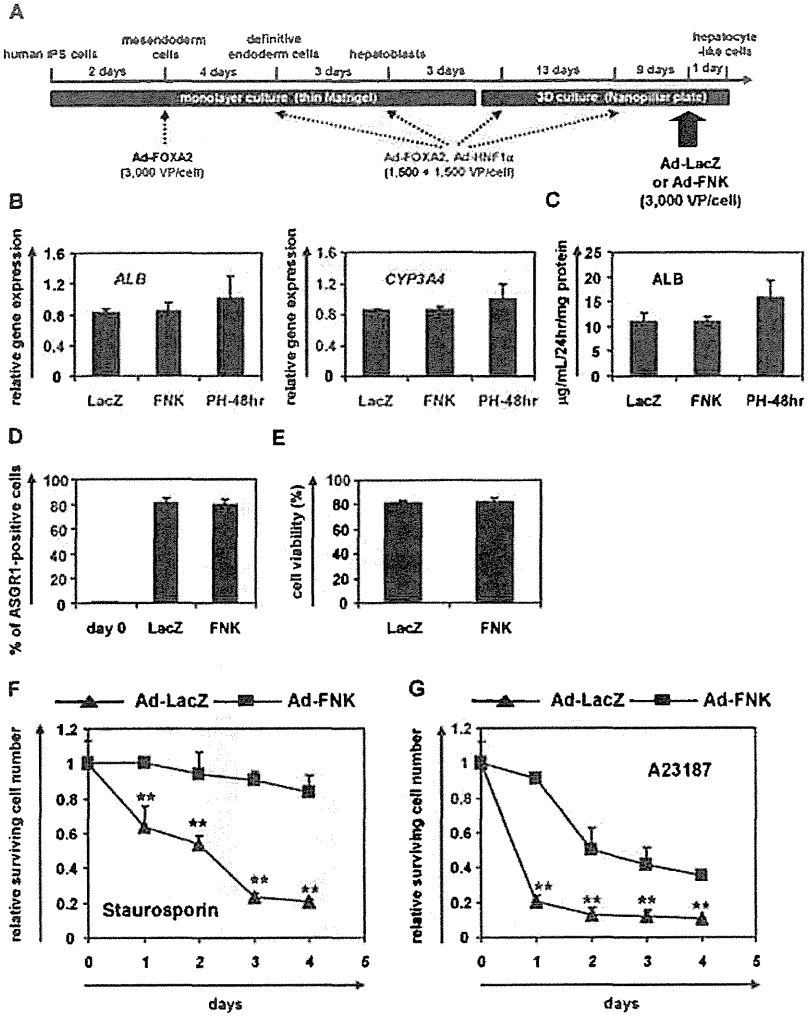

190x254mm (72 x 72 DPI)

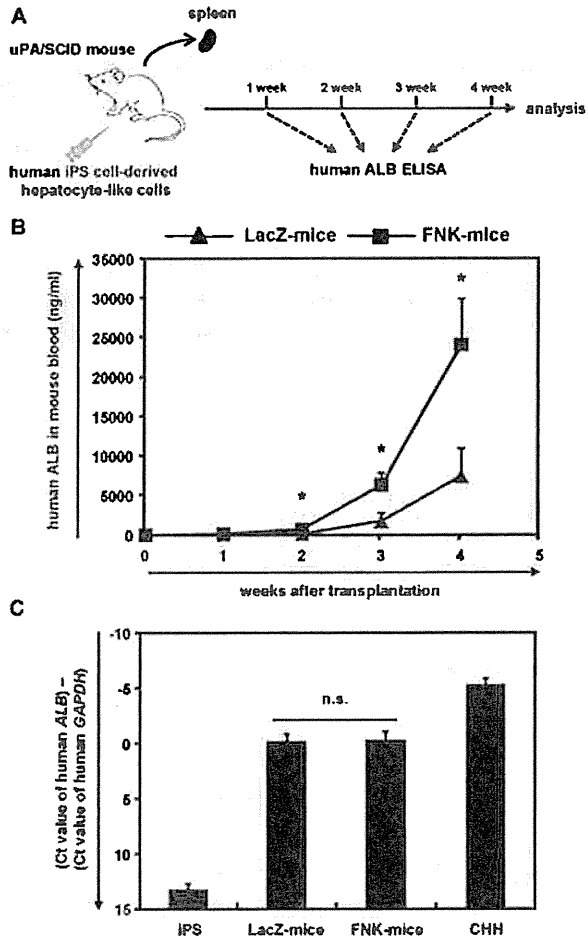

190x254mm (72 x 72 DPI)

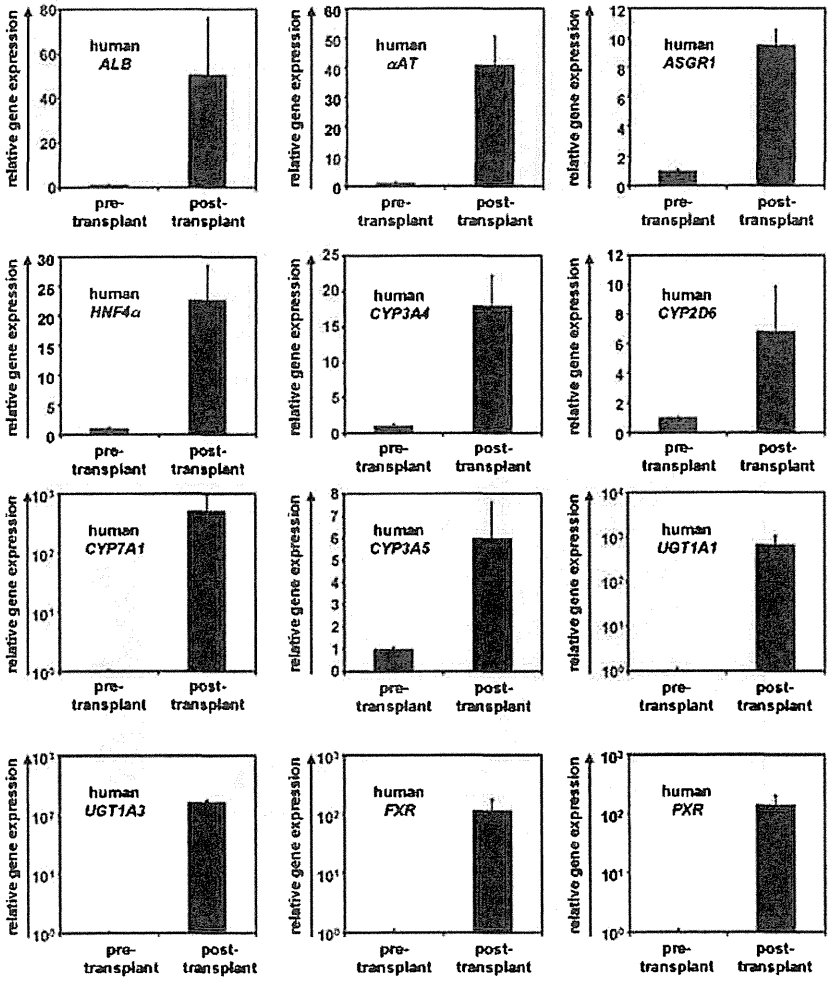

190x254mm (72 x 72 DPI)

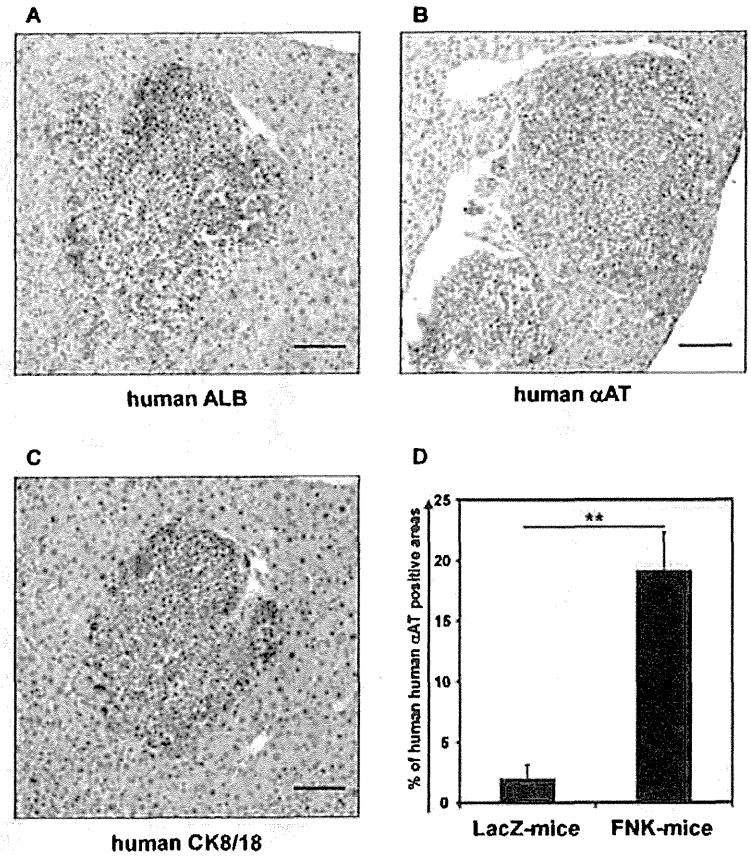

190x254mm (72 x 72 DPI)

Hepatology Research

Hepatology Research 2014; 44: 460–473 doi: 10.1111/hepr.12140

Original Article

Cilostazol attenuates hepatic stellate cell activation and protects mice against carbon tetrachloride-induced liver fibrosis

Shunichi Saito,[1] Koichiro Hata,[1] Keiko Iwaisako,[1,3] Atsuko Yanagida,[1] Masatoshi Takeiri,[2] Hirokazu Tanaka,[1] Shoichi Kageyama,[1] Hirofumi Hirao,[1] Kazuo Ikeda,[3] Masataka Asagiri[2] and Shinji Uemoto[1]

[1]Department of Surgery, Division of Hepato-Pancreato-Biliary Surgery and Transplantation, and [2]Innovation Center for Immunoregulation and Therapeutics, Graduate School of Medicine, Kyoto University, Kyoto, and [3]Department of Anatomy and Regenerative Biology, Graduate School of Medicine, Osaka City University, Osaka, Japan

Aim: Liver fibrosis is a common pathway leading to cirrhosis. Cilostazol, a clinically available oral phosphodiesterase-3 inhibitor, has been shown to have antifibrotic potential in experimental non-alcoholic fatty liver disease. However, the detailed mechanisms of the antifibrotic effect and its efficacy in a different experimental model remain elusive.

Methods: Male C57BL/6J mice were assigned to five groups: mice fed a normal diet (groups 1 and 2); 0.1% or 0.3% cilostazol-containing diet (groups 3 and 4, respectively); and 0.125% clopidogrel-containing diet (group 5). Two weeks after feeding, groups 2–5 were intraperitoneally administered carbon tetrachloride (CCl_4) twice a week for 6 weeks, while group 1 was treated with the vehicle alone. To investigate the effects of cilostazol on hepatic cells, *in vitro* studies were conducted using primary hepatic stellate cells (HSC), Kupffer cells and hepatocytes with cilostazol supplementation.

Results: Sirius red staining revealed that groups 3 and 4 exhibited a lesser fibrotic area (2.49 ± 0.43% and 2.31 ± 0.30%, respectively) than group 2 (3.17 ± 0.67%, $P < 0.05$ and $P < 0.001$, respectively). *In vitro* studies showed cilostazol dose-dependently suppressed HSC activation (assessed by morphological change, cell proliferation, and the expression of HSC activation markers), suggesting the therapeutic effect of cilostazol is mediated by its direct action on HSC.

Conclusion: Cilostazol could alleviate CCl_4-induced hepatic fibrogenesis *in vivo*, presumably due, at least partly, to its direct effect to suppress HSC activation. Given its clinical availability and safety, it may be a novel therapeutic intervention for chronic liver diseases.

Key words: carbon tetrachloride, cilostazol, hepatic stellate cells, liver fibrosis, phosphodiesterase-3 inhibitor, platelet-derived growth factor

Correspondence: Dr Koichiro Hata, Department of Surgery, Division of Hepato-Pancreato-Biliary Surgery and Transplantation, Graduate School of Medicine, Kyoto University, Kyoto 606-8507, Japan.
Email: khata@kuhp.kyoto-u.ac.jp; Dr Masataka Asagiri, Innovation Center for Immunoregulation and Therapeutics, Graduate School of Medicine, Kyoto University, Kyoto 606-8501, Japan.
Email: masa-asagiri@umin.org

Conflict of interest: Drs Hata and Uemoto receive a grant from Otsuka Pharma. Dr Asagiri receives a grant from the AK Project (between Astellas Pharma and Kyoto University). However, the study was designed, conducted, analyzed, and reported independently of the funding agencies and pharmaceutical companies, although cilostazol was supplied by Otsuka Pharmaceutical. No other potential conflict of interest relevant to this article was reported.
Received 17 August 2012; revision 8 April 2013; accepted 15 April 2013.

INTRODUCTION

LIVER FIBROSIS, A precursor to cirrhosis, is a common consequence of almost all types of chronic liver injuries, including viral, alcoholic, autoimmune, metabolic and drug-induced liver diseases.[1] Fibrosis results from excessive accumulation of extracellular matrix (ECM) components, such as collagen type I. Left untreated, fibrosis can progress to liver cirrhosis and ultimately lead to organ failure and death. The activation of hepatic stellate cells (HSC) in response to liver injury is considered to be an essential event underlying hepatic fibrogenesis.[2–4] The activation of HSC refers to the trans-differentiation of quiescent HSC into proliferative and contractile myofibroblast-like cells. These activated HSC

secrete excess ECM proteins and contribute to the development of hepatic fibrosis. Several types of growth factors, cytokines, chemokines and their cognate receptors are associated with HSC activation. Among these, transforming growth factor (TGF)-β1 and platelet-derived growth factor (PDGF) are probably the most important.[5–7] HSC play a key role in liver fibrosis, thereby restraining the activation of HSC may attenuate liver fibrosis. Thus, numerous studies have attempted to suppress HSC activation in order to develop new treatment strategies for hepatic fibrosis.[8–11] Cilostazol (OPC-13013 [6-[4-[1-cyclohexyl-1H-tetrazol-5-yl]butoxy]-3,4-dihydro-2[1H]-quinolinone]) is a synthetic vasodilator and an antiplatelet agent. It was approved in 1988 in Japan for the treatment of symptoms related to occlusive peripheral arterial disease (Pletaal; Otsuka Pharmaceutical Co., Ltd., Tokyo, Japan) and subsequently in 1999 in the USA and in 2001 in the UK (Pletal; Otsuka America Pharmaceutical, Inc., Rockville, MD, USA and Otsuka Pharmaceutical Europe Ltd., Uxbridge, UK) for the treatment of intermittent claudication symptoms.[12–14] Over the past 20 years, it has been widely used as a potent inhibitor of platelet aggregation and thrombosis.[15–18] It has also been shown to inhibit PDGF secretion *in vitro*.[19] The antiplatelet activity of cilostazol is attributed to its inhibition of cyclic adenosine monophosphate (cAMP) phosphodiesterase (PDE). Recent studies have identified 11 different families of PDE. Of these, cilostazol selectively inhibits PDE3, which is predominantly expressed in platelets, vascular smooth muscle cells, cardiac myocytes and hepatic cells.[20,21] Recently, increased intracellular cAMP has been shown to inhibit HSC activation,[22–25] although little is known about the effect of cilostazol on liver fibrosis. Furthermore, cilostazol was shown to have an antifibrotic potential in experimental non-alcoholic fatty liver disease.[26] However, the precise mechanisms of the antifibrotic effect and its efficacy in a different experimental model are elusive. This study was designed to investigate the effect of cilostazol on carbon tetrachloride (CCl_4)-induced hepatic fibrogenesis in mice and to clarify its mechanism of action by pathological examination and analysis of primary cells derived from the mice.

METHODS

Animals

MALE C57BL/6J MICE aged 4 weeks were purchased from Japan SLC (Shizuoka, Japan). After an acclimation period of 7 days, the mice were randomly assigned to the five treatment groups ($n = 10$ per group) in a single-blinded fashion (Fig. 1). The mice were maintained on standard chow and allowed free access to food and water. The protocol for animal handling was reviewed and approved by the Animal Care and Use Committee of Kyoto University.

Mouse model of liver fibrosis

Two weeks after assignment to treatment groups, the mice were treated with CCl_4 (2 μL/g bodyweight diluted 1:4 in corn oil) by intraperitoneal (i.p.) injection twice a week for 6 weeks. The mice were sacrificed 4 days after the last injection.

Drugs and drug treatment

The antiplatelet drug cilostazol was a gift from Otsuka Pharma (Tokushima, Japan). Clopidogrel was purchased from Sanofi-Aventis (Tokyo, Japan). Each drug was administrated in standard pellet food (Oriental Bio Service, Kyoto, Japan) containing cilostazol (0.1% w/w), cilostazol (0.3% w/w) or clopidogrel (0.125% w/w). Oral treatment with cilostazol at 0.1% and 0.3% w/w, and clopidogrel at 0.125% w/w of chow is equivalent to the clinically used doses.[27–29] The alternative antiplatelet drug clopidogrel was used as a control. To raise and stabilize the plasma concentration of the drugs, the animals were pretreated with the drugs for 2 weeks. All animals were closely observed for 2 weeks after the dietary change, and then received CCl_4 injections for 6 weeks. The food intake and bodyweight changes were monitored throughout the experimental period for 8 weeks. Blood samples were collected from the inferior vena cava of the mice, and liver weights were recorded at death.

Histological examination and immunohistochemistry

For histological evaluation, the right lobe of the liver of each mouse was collected at death and fixed in 4% paraformaldehyde (PFA). In order to assess fibrosis, paraffin-embedded sections were stained with picrosirius red (Sigma, St Louis, MO, USA).[30] Expression levels of α-smooth muscle actin (α-SMA) and F4/80 were immunohistochemically determined in paraffin-embedded sections as described previously[31] using a monoclonal antimouse α-SMA antibody (1:300, clone: 1A4; Dako, Glostrup, Denmark) or anti-mouse F4/80 antibody (1:100, clone: BM8; eBioscience, San Diego, CA, USA), respectively.

Sirius red-positive areas, α-SMA-positive areas and F4/80-positive areas were quantified from 10 random ×100 fields from each animal ($n = 10$ per treatment

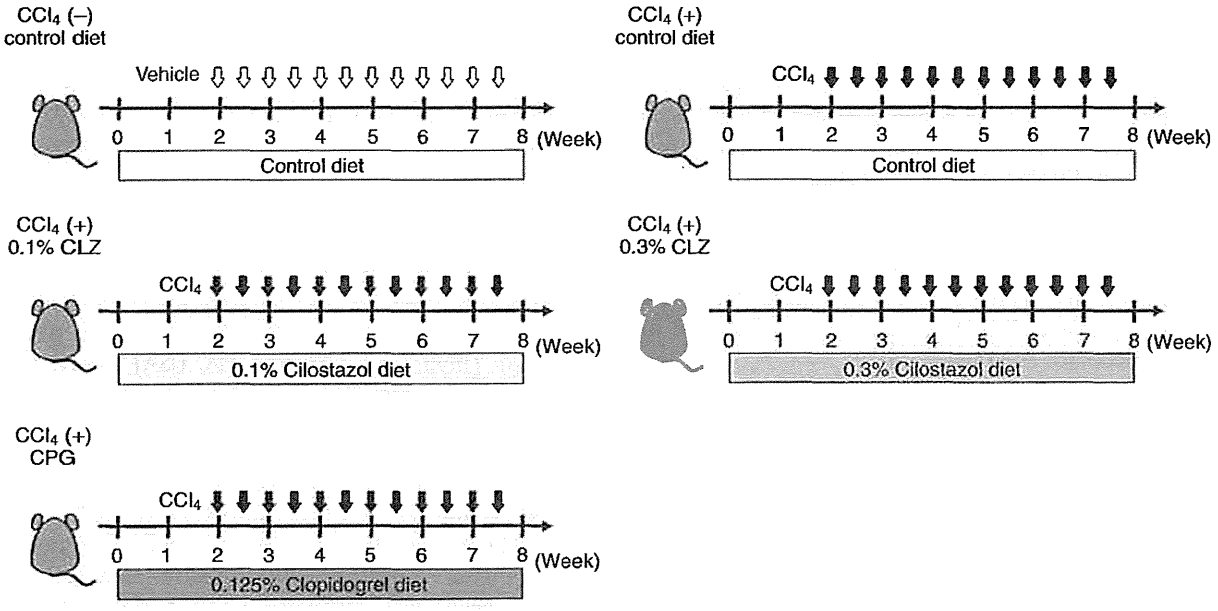

Figure 1 Experimental protocol. Male adult C57BL/6J mice were fed pelleted food containing 0.1% or 0.3% cilostazol or 0.125% clopidogrel, or fed a control diet. Liver fibrosis was induced by i.p. injection of CCl_4 twice a week for 6 weeks. Mice were killed 4 days after the last injection. CLZ, cilostazol; CPG, clopidogrel; CCl_4, carbon tetrachloride. ($n = 10$). ⇩, vehicle i.p.; ⬇, CCl_4, 0.5 μL/g bodyweight i.p.

group) using image processing software (BZ analyzer; Keyence, Osaka, Japan). Data are presented as the percentage area positively stained for Sirius red, α-SMA or F4/80.

Measurement of hepatic collagen content

For measurement of liver fibrosis, the specific amino acid of collagen type I, hydroxyproline, was quantified in liver tissue. The hepatic hydroxyproline content was measured as previously described.[32] In brief, liver tissue was homogenized in 900 μL of ice-cold distilled water. Subsequently, 125 μL of 50% trichloroacetic acid was added, and the homogenates were incubated on ice for 20 min. Precipitated pellets were hydrolyzed for 18 h at 110°C in 6 N HCl. After hydrolysis, the samples were filtered and neutralized with 10 N NaOH, and hydrolysates were oxidized with chloramine-T (Sigma) for 25 min at room temperature. The reaction mixture was then incubated in Ehrlich's perchloric acid solution at 65°C for 20 min and then cooled to room temperature. Sample absorbance was measured at 560 nm in duplicate. Purified hydroxyproline (Sigma) was used as a standard. The hydroxyproline content was expressed as nanograms of hydroxyproline per gram of liver.

Immunoblot analysis

For analysis of α-SMA protein expression, immunoblotting was performed with whole liver lysates (20 μg/lane) using standard techniques. Immunoblotting was performed using a polyclonal antigoat glyceraldehyde 3-phosphate dehydrogenase (GAPDH) antibody (1:200; #sc-20357; Santa Cruz Biotechnology, Santa Cruz, CA, USA) as an internal control, a polyclonal antirabbit α-SMA antibody (1:200; #ab-5694; Abcam, Cambridge, UK) and horseradish peroxidase-conjugated secondary antibodies (Santa Cruz Biotechnology) as described in the manufacturer's protocol.[33] Antibody staining was visualized with an enhanced chemiluminescence system (GE Healthcare Biosciences, Little Chalfont, UK) using Lumino-image analyzer (LAS-3000 mini; Fujifilm, Tokyo, Japan). Band density was quantified from digital images using ImageJ software.

Isolation and culture of hepatic cells

Primary HSC, Kupffer cells and hepatocytes were isolated from the mouse liver as described previously.[34–36] In brief, HSC and Kupffer cells were isolated from mice by two-step collagenase–pronase perfusion followed by three-layer discontinuous density gradient

centrifugation with 8.2% (w/v) and 14.5% (w/v) Nycodenz (Accurate Chemical and Scientific, Westbury, NY, USA) to obtain HSC and Kupffer cell fractions. HSC were collected between the 0% and 8.2% (w/v) layer. Kupffer cells were collected between the 8.2% and 14.5% (w/v) layers and purified by differential plating. HSC and Kupffer cells were cultured in Dulbecco's modified Eagle's medium (DMEM; Sigma) supplemented with 10% fetal bovine serum (FBS) and antibiotics. Hepatocytes were cultured in William's medium E supplemented with 10% FBS and antibiotics on the collagen-coated dish. Hepatic cells were cultured in a CO_2 incubator at 37°C.

Cilostazol treatment

Cilostazol was dissolved in dimethylsulfoxide and diluted in DMEM supplemented with 10% FBS and antibiotics. Complete medium containing final concentration of 0 μM (control), 5 μM and 15 μM cilostazol was added to cultures 1 day after isolation.

Measurement of Intracellular cAMP

The intracellular cAMP level was measured as described previously[37] using the cAMP-Glo max assay kit (Promega, Madison, WI, USA). Briefly, 1×10^4 cells were seeded in a 96-well plate with or without cilostazol in culture medium containing 10% FBS and incubated at 37°C for 24 h. The cAMP detecting solution was added to each well and incubated at room temperature for 20 min. The Kinase-Glo reagent was added to each well. The plate was shaken for 1 min at room temperature and incubated at room temperature for 10 min. Finally, the luminescent signal was measured by a plate reader (Arvo; Perkin-Elmer, Waltham, MA, USA).

Time-lapse recording and cell counting

For the observation of morphological changes, HSC were placed in a Lab-Tek plastic four-well chamber slide (Nunc, Naperville, IL, USA) and maintained at 37°C in 10% CO_2. Time-lapse images were taken using an inverted microscope (BZ9000; Keyence, Osaka, Japan) over 6 days following cilostazol treatment. Cells were counted in four random ×200 fields on each chamber using BZ analyzer image processing software.

Cytochemical analysis

Primary HSC in each chamber were fixed in 10% formalin/PBS for 10 min blocked with Dako Protein Block (#X0909; Dako, Glostrup, Denmark) for 1 h, incubated overnight with a polyclonal antimouse α-SMA antibody (1:200; #A2524, Sigma) in a blocking solution, washed with PBS, and incubated with Alexa Flour 594 goat antimouse immunoglobulin G (1:600; #A-11005; Invitrogen, San Diego, CA, USA) secondary antibody and 4′,6′-diamidino-2-phenylindole dihydrochloride (DAPI) nuclear stain for 1 h. Finally, HSC were washed and observed with an inverted fluorescence microscope, BZ9000 (Keyence).

Reverse-transcriptase quantitative polymerase chain reaction (RT–qPCR)

For gene expression analysis, total RNA was extracted from liver tissue, HSC or Kupffer cells using TRIZOL reagent (Invitrogen, Carlsbad, CA, USA) according to the manufacturer's protocol. DNase-treated RNA was reverse transcribed using the Omniscript RT Kit (Qiagen, Hilden, Germany) according to the manufacturer's protocol. RT-qPCR was performed for 55 cycles of 15 s at 95°C and 60 s at 60°C using SYBR Green I Kits for the LightCycler 480 instrument (Roche Diagnostics, Mannheim, Germany). The relative abundance of target genes was calculated using a standard curve normalized to α-tubulin or 18S. Probes and primers for α-SMA (NM_007392), collagen α1 (I) (NM_007742), PDGF-B (NM_011057), PDGF receptor (PDGFR)-β (NM_008809), TGF-β1 (NM_011577), TGF-βR1 (NM_009370), tumor necrosis factor (TNF)-α (NM_013693), interleukin (IL)-1β (NM_008361), monocyte chemotactic protein (MCP)1 (NM_011333), F4/80 (NM_010130), 18S (NR_003278) and α-tubulin (NM_011653) were designed by and purchased from Life Technologies (Carlsbad, CA, USA).

Statistical analysis

Results are reported as mean ± 95% confidence intervals (CI). Statistical comparisons were made using Student *t*-test or two- or one-way ANOVA followed by Bonferroni's post-hoc test. $P < 0.05$ was considered to be significant.

RESULTS

Cilostazol alleviated fibrous change in the liver

IN ORDER TO validate the antifibrotic efficacy of cilostazol, we utilized a widely used experimental mouse model of liver fibrosis induced by CCl_4 injections (twice a week for 6 weeks; Fig. 1). Based on the pharmacokinetic data of the plasma concentration of the drugs, 0.1% and 0.3% cilostazol and 0.125% clopidogrel were used as clinically equivalent doses. Collagen deposition, a marker for liver fibrosis, was assessed by Sirius red

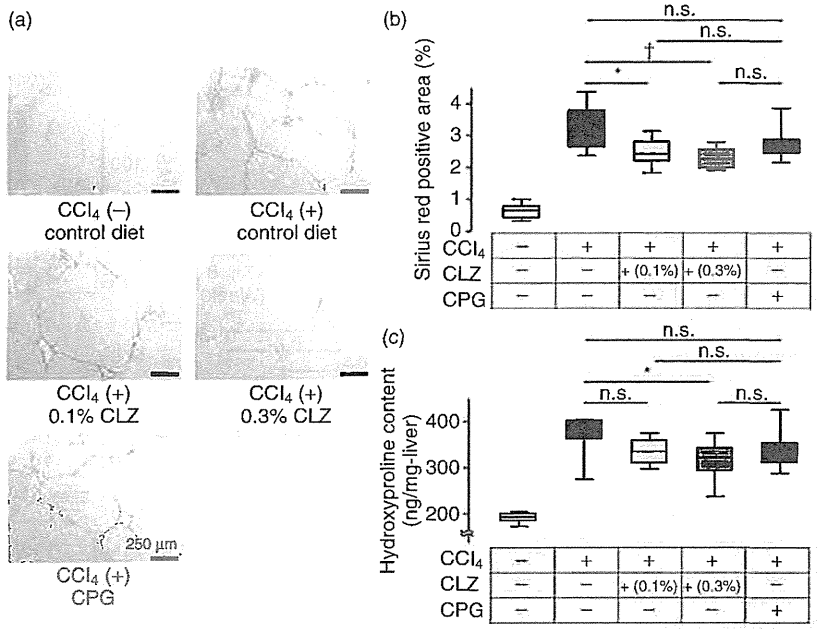

Figure 2 Cilostazol alleviated fibrous changes in the liver. (a) Sirius red staining of liver sections in each group. CCl_4 treatment for 6 weeks remarkably increased the fibrotic area. CCl_4-treated liver in the control or clopidogrel-administrated group showed bridging fibrosis. Cilostazol decreased the fibrotic area among CCl_4-treated mice (original magnification ×100). (b) Quantification of liver fibrosis area stained by Sirius red. CCl_4-induced fibrous areas in the 0.1% or 0.3% cilostazol-administrated groups were significantly decreased compared with that in the control group. (c) Hydroxyproline assay was performed to measure the total collagen content. Administration with 0.3% cilostazol reduced tissue hydroxyproline levels compared with control. The box plots present the median and 25th–75th percentiles. Upper and lower lines represent the minimum and maximum values ($n = 10$). *$P < 0.05$; †$P < 0.001$ vs CCl_4-treated control. CCl_4, carbon tetrachloride; CLZ, cilostazol; CPG, clopidogrel.

staining (Fig. 2a). Sirius red staining of the liver in the 0.1% and 0.3% cilostazol-administrated groups (2.49%; 95% CI = 2.18–2.80; and 2.31%; 95% CI = 2.10–2.52) was significantly lower than in the control group (3.17%; 95% CI = 2.70–3.65; $P < 0.05$ and $P < 0.001$, respectively), however, clopidogrel had no effect (Fig. 2a,b). This was reflected by hydroxyproline content, which was significantly reduced in the 0.3% cilostazol-administrated group (317 ng/mg liver; 95% CI = 289–346) compared with that in the control group (371 ng/mg liver; 95% CI = 344–398; $P < 0.001$; Fig. 2c). Thus, p.o. administration of cilostazol reduces hepatic fibrogenesis at clinical doses. During the 8-week experimental duration, no significant difference in bodyweight change or peripheral platelet count was observed among treatment groups (Fig. 3a,b), indicating minimal toxicity of the drugs. Moreover, there was no apparent difference in CCl_4-induced hepatocyte damage among the groups, as assessed by peripheral blood aspartate aminotransferase and alanine aminotransferase levels (Fig. 3c,d) and hematoxylin–eosin staining (Fig. 3e). We also observed no morphological change in cultured primary hepatocytes supplemented with cilostazol (Fig. 3f).

Cilostazol attenuated the activation of HSC in the liver

Chronic liver injury can lead to unrestrained HSC activation, resulting in excessive production of extracellular matrices and hepatic fibrosis. Thus, we assessed the activation status of HSC in the liver, by immunohistochemical staining of α-SMA, a marker of HSC activation (Fig. 4a). Similar to the Sirius red staining data, the α-SMA positive area in the liver of the 0.1% (4.16%; 95% CI = 3.17–5.15) and 0.3% (2.61%; 95% CI = 2.17–3.05) cilostazol-administrated groups was clearly reduced in a dose-dependent manner compared with the control group (7.13%; 95% CI = 4.10–10.2; $P < 0.05$ and $P < 0.001$, respectively; Fig. 4b) and clopidogrel-administrated animals. This result was also reflected by immunoblotting experiments in which α-SMA protein expression was significantly reduced in

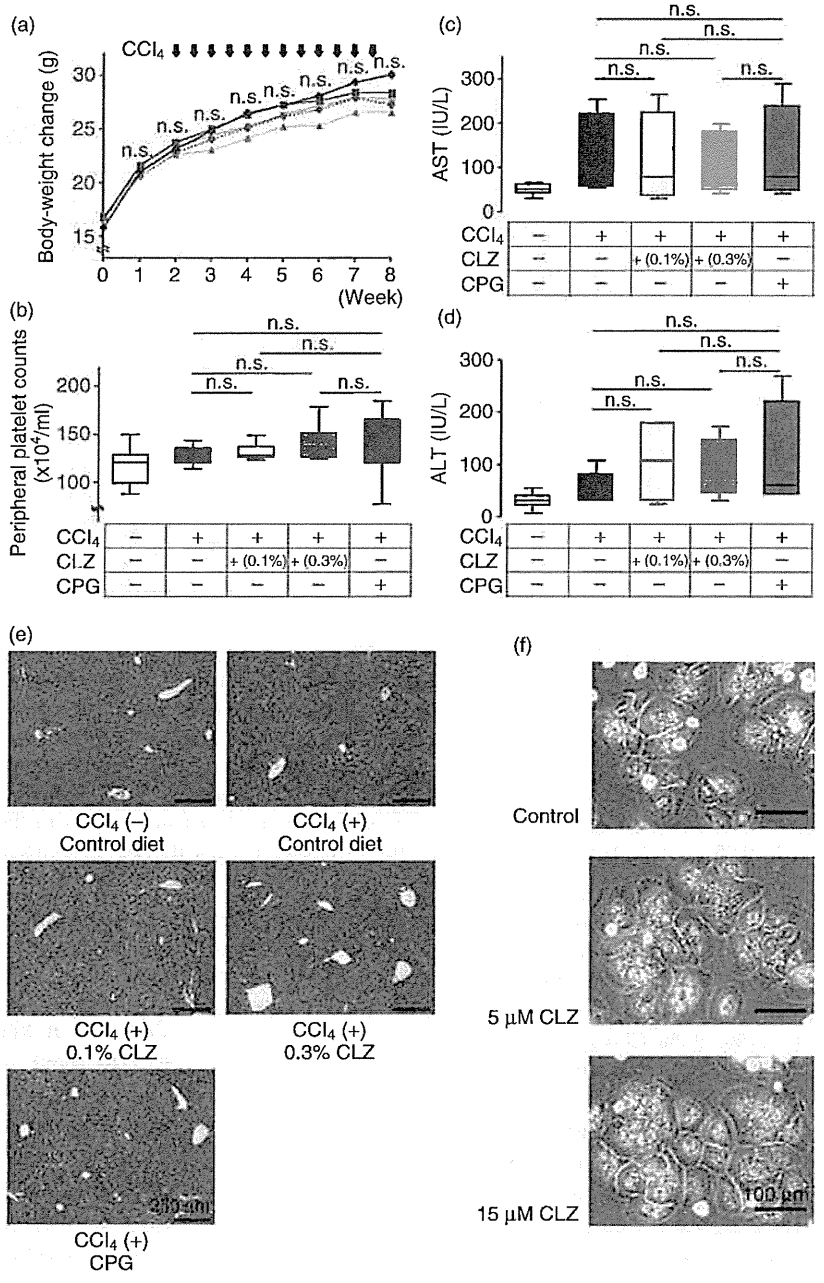

Figure 3 Bodyweight change, peripheral platelet counts, hepatocyte damage and aspartate aminotransferase (AST)/alanine aminotransferase (ALT) did not differ among the CCl_4-treated groups. (a) Bodyweight change during the 8-week experimental duration. Mice without CCl_4 treatment showed the highest gain, however, no significant differences were observed among groups. (b) Peripheral platelet counts at death were not different among CCl_4-treated groups. (c,d) Serum AST and ALT levels at death were not different among CCl_4-treated groups. (e) Hematoxylin–eosin staining of liver sections from each group (original magnification ×100). No obvious differences in hepatocyte damage existed among CCl_4-treated groups. (f) Morphology of hepatocytes supplemented with cilostazol for 1 day was observed under a phase contrast microscope (original magnification ×200). The morphology was unaffected by cilostazol supplementation. On line plots, each plot represents the mean of measurements ($n = 10$). The box plots present the median and 25th–75th percentiles. Upper and lower lines represent the minimum and maximum values ($n = 10$). CCl_4, carbon tetrachloride; CLZ, cilostazol; CPG, clopidogrel. –◆–, CCl_4 (–) + control diet; –■–, CCl_4 (+) + 0.3% cilostazol; –■–, CCl_4 (+) + 0.1% cilostazol; –◆–, CCl_4 (+) + control diet; –▲–, CCl_4 (+) + clopidogrel.

the 0.3% cilostazol-administrated group (0.44%; 95% CI = 0.29–0.60) compared with that in the control group (1.14%; 95% CI = 0.55–1.72; $P < 0.05$; Fig. 4c). These results indicate that cilostazol has potent activity to attenuate HSC activation in the liver through unknown mechanisms.

Cilostazol directly and effectively inhibits the activation of HSC but not of Kupffer cells

To reveal the possible mechanisms underlying these *in vivo* observations, we performed *in vitro* studies in